

# Dynamic regulation of human endogenous retroviruses mediates factor-induced reprogramming and differentiation potential

Mari Ohnuki<sup>a,1</sup>, Koji Tanabe<sup>a,2</sup>, Kenta Sutou<sup>a</sup>, Ito Teramoto<sup>a</sup>, Yuka Sawamura<sup>a</sup>, Megumi Narita<sup>a</sup>, Michiko Nakamura<sup>a</sup>, Yumie Tokunaga<sup>a</sup>, Masahiro Nakamura<sup>a</sup>, Akira Watanabe<sup>a</sup>, Shinya Yamanaka<sup>a,b,3</sup>, and Kazutoshi Takahashi<sup>a,3</sup>

<sup>a</sup>Center for iPSC Cell Research and Application, Kyoto University, Kyoto 606-8507, Japan; and <sup>b</sup>Gladstone Institute of Cardiovascular Disease, San Francisco, California 94158

Contributed by Shinya Yamanaka, July 14, 2014 (sent for review June 6, 2014; reviewed by Konrad Hochedlinger)

Pluripotency can be induced in somatic cells by overexpressing transcription factors, including POU class 5 homeobox 1 (OCT3/4), sex determining region Y-box 2 (SOX2), Krüppel-like factor 4 (KLF4), and myelocytomatosis oncogene (c-MYC). However, some induced pluripotent stem cells (iPSCs) exhibit defective differentiation and inappropriate maintenance of pluripotency features. Here we show that dynamic regulation of human endogenous retroviruses (HERVs) is important in the reprogramming process toward iPSCs, and in re-establishment of differentiation potential. During reprogramming, OCT3/4, SOX2, and KLF4 transiently hyperactivated LTR7s—the long-terminal repeats of HERV type-H (HERV-H)—to levels much higher than in embryonic stem cells by direct occupation of LTR7 sites genome-wide. Knocking down LTR7s or long intergenic non-protein coding RNA, regulator of reprogramming (*lincRNA-RoR*), a HERV-H-driven long noncoding RNA, early in reprogramming markedly reduced the efficiency of iPSC generation. KLF4 and LTR7 expression decreased to levels comparable with embryonic stem cells once reprogramming was complete, but failure to resuppress KLF4 and LTR7s resulted in defective differentiation. We also observed defective differentiation and LTR7 activation when iPSCs had forced expression of KLF4. However, when aberrantly expressed KLF4 or LTR7s were suppressed in defective iPSCs, normal differentiation was restored. Thus, a major mechanism by which OCT3/4, SOX2, and KLF4 promote human iPSC generation and reestablish potential for differentiation is by dynamically regulating HERV-H LTR7s.

retrotransposon | epigenetics | evolution

Human pluripotent stem cells can be generated through two paths: (i) embryonic stem cells (ESCs) can be derived from embryos (1), and (ii) induced pluripotent stem cells (iPSCs) can be generated from differentiated cells through factor-mediated reprogramming (2). Most iPSCs are highly similar to ESCs, but we recently showed that ~10% of iPSC clones have a differentiation-defective phenotype, such that 20% of cells were undifferentiated, even after in vitro-directed neural differentiation (3). These differentiation-defective (DD)-iPSC clones exhibited high expression levels of ~10 genes—including abhydrolase domain containing 12B (*ABHD12B*), HERV-H LTR-associating 1 (*HHLA1*) and chromosome 4 open reading frame 51 (*C4ORF51*)—driven by the long-terminal repeats (LTRs) of human endogenous retroviruses (HERVs).

HERVs constitute ~8% of the human genome as a result of their transposon activity, but they can no longer perform transposition (4). HERV type-H (HERV-H) transcripts are expressed in ESCs/iPSCs at higher levels than in differentiated cells (5). Approximately 80% of the LTRs belonging to the 50 most highly expressed HERV-H proviruses are occupied by core transcription factors involved in pluripotency, including POU class 5 homeobox 1 (OCT3/4), sex determining region Y-box 2 (SOX2), and NANOG homeobox (NANOG). Furthermore, HERV-H proviruses are expressed less in some iPSCs than in other iPSCs

and ESCs, suggesting that HERV-H expression may be a barometer of pluripotency (5). Species-specific transposable elements, including HERVs, contribute up to 25% of the core transcription-factor binding sites in mouse and human pluripotent stem cells, wiring new genes into the core regulatory network of pluripotency in each species (6). These observations suggest that transposable elements may be important determinants of pluripotency. However, little is known about the roles of HERVs in reprogramming during iPSC generation.

In the present study, we found that during reprogramming of somatic cells toward iPSCs, HERV-H LTR7s were transiently activated to levels much higher than in ESCs, and this transient activation was required for efficient reprogramming. When reprogramming was

## Significance

In this study, we found that human endogenous retroviruses type-H (HERV-Hs) are transiently hyperactivated during reprogramming toward induced pluripotent stem cells (iPSCs) and play important roles in this process. However, when reprogramming is complete and cells acquire full pluripotency, HERV-H activity should decrease to levels comparable with those in embryonic stem cells because failure to resile this activity leads to the differentiation-defective phenotype in neural lineage. We also found that during reprogramming, reprogramming factors, including POU class 5 homeobox 1 (OCT3/4), sex determining region Y-box 2 (SOX2), and Krüppel-like factor 4 (KLF4) (OSK) bind to and activate long-terminal repeats of HERV-Hs. KLF4 possibly precludes Tripartite motif containing 28 and recruits not only OCT3/4 and SOX2, but also E1A binding protein p300 (p300) histone acetyltransferase on HERV-H loci. Therefore, OKSM-induced HERV-H activation constitutes an unanticipated and critical mechanism for iPSC formation.

Author contributions: S.Y. and K. Takahashi designed research; M.O., K. Tanabe, K.S., I.T., Y.S., M. Narita., Michiko Nakamura, and K. Takahashi performed research; M.O., Y.T., Masahiro Nakamura, A.W., and K. Takahashi analyzed data; K. Tanabe contributed new reagents/analytic tools; and S.Y. and K. Takahashi wrote the paper.

Reviewers included: K.H., Howard Hughes Medical Institute and Massachusetts General Hospital Cancer Center.

Conflict of interest statement: S.Y. is a member without salary of the scientific advisory board of iPSC Academia Japan.

Freely available online through the PNAS open access option.

Data deposition: The data reported in this paper have been deposited in the Gene Expression Omnibus (GEO) database, [www.ncbi.nlm.nih.gov/geo](http://www.ncbi.nlm.nih.gov/geo) (accession nos. GSE54848 and GSE56569).

<sup>1</sup>Present address: Anthropology and Human Genetics Department Biology II, Ludwig Maximilians University Munich, 82152 Martinsried, Germany.

<sup>2</sup>Present address: Institute for Stem Cell Biology and Regenerative Medicine, Stanford School of Medicine, Stanford, California 94305.

<sup>3</sup>To whom correspondence may be addressed. Email: [yamanaka@cira.kyoto-u.ac.jp](mailto:yamanaka@cira.kyoto-u.ac.jp) or [takahash@cira.kyoto-u.ac.jp](mailto:takahash@cira.kyoto-u.ac.jp).

This article contains supporting information online at [www.pnas.org/lookup/suppl/doi:10.1073/pnas.1413299111/-DCSupplemental](http://www.pnas.org/lookup/suppl/doi:10.1073/pnas.1413299111/-DCSupplemental).

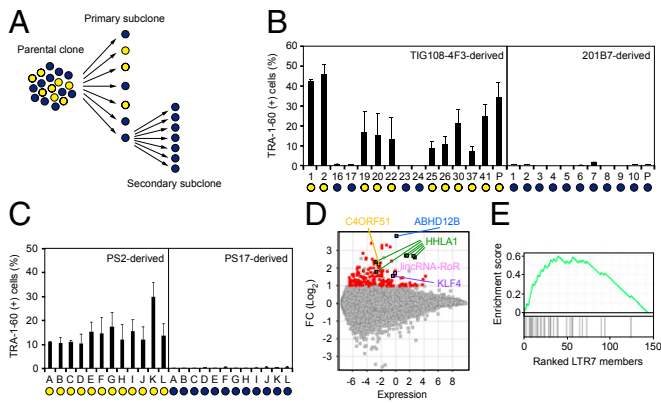


**Fig. 1.** Enrichment of LTR7s in subcloned DD-iPSCs. (A) Summary of single-cell subcloning. (B) Differentiation potential of primary subclones. Shown are the percentages of TRA-1-60 (+) cells 14 d after neural induction of each primary subclone analyzed by flow cytometry. Blue and yellow circles indicate normal and DD-iPSC subclones/parents, respectively.  $n = 3$ . Error bars are SDs. (C) Differentiation potential of secondary subclones. Shown are the percentages of TRA-1-60 (+) cells 14 d after neural induction of TIG108-4F3-PS2- and PS17-derived secondary subclones. Blue and yellow circles indicate normal and DD-iPSC subclones, respectively.  $n = 3$ . Error bars are SDs. (D) Differential expression of genes between normal and DD-iPSCs. MA plot comparing global gene expression in normal ( $n = 18$ ) and DD ( $n = 37$ ) primary subclones derived from four DD-iPSCs parental clones (TIG108-4F3, TIG118-4F1, 451F3, and TKCBV5-6). Red and colored dots indicate genes with significantly higher expression in DD-iPSCs ( $FC > 2$ ,  $FDR < 0.05$ ). (E) Correlation between DD-marker expression and the presence of LTR7 elements. GSEA plot showing enrichment of LTR7 elements in 144 DD-iPSC markers. DD-iPSC markers are displayed in order of their fold-changes between normal- ( $n = 18$ ) and DD- ( $n = 37$ ) iPSC subclones in expression levels determined by a microarray.

complete, HERV-H expression decreased to levels comparable with those in ESCs. However, in DD-iPSC clones, HERV-H LTR7s remained aberrantly activated, leading to the defective differentiation. Thus, transient hyperactivation of HERVs is important in reprogramming somatic cells toward pluripotency and establishment of differentiation potential, revealing a previously unrecognized mechanism critical to cellular reprogramming technology.

## Results

**Characteristics of DD-iPSCs.** To better understand the nature of DD-iPSCs, we performed single-cell subcloning with four defective iPSC lines established using retroviral vectors, such as TKCBV5-6 (7), TIG108-4F3 (3), and TIG118-4F1 (3), and integration-free episomal vectors, such as 451F3 (8) (Fig. 1A). The subclones were identical to their parental clones regarding patterns of integrated retroviral vectors and short tandem repeats (Fig. S1A and Dataset S1). Based on marker-gene expression and neural differentiation potential, each DD-iPSC subclone had a normal or DD phenotype, whereas all subclones derived from ESCs and normal iPSCs exhibited a normal phenotype (3, 9) (Fig. 1B and Fig. S1B). The primary DD subclones derived from TIG108-4F3 DD-iPSCs were then used to produce secondary subclones, all of which showed the DD phenotype. Similarly, all normal primary subclones produced only normal secondary subclones (Fig. 1C). These data demonstrate that each DD-iPSC parental clone is monoclonal but consists of both DD and normal iPSCs. However, the DD phenotype is stable once subclones are isolated.

The subcloning experiments allowed us to compare DD-iPSCs and their normal counterparts under the same genetic background. Microarray comparison of global gene expression in normal and DD-iPSC subclones identified 144 marker genes that were enriched in DD-iPSCs (Fig. 1D and Dataset S2), including the three previously reported genes *ABHD12B*, *HHLA1*, and *C4ORF51*. We also identified long intergenic non-protein coding RNA, regulator of

reprogramming (*lincRNA-RoR*), an HERV-H LTR7-related large intergenic noncoding RNA (*lincRNA*), and *KLF4* as DD-iPSC marker genes (3, 10). Of the DD-iPSC markers, 21.5% (31 of 144) were located within 30 kb downstream of LTR7s. Gene set enrichment analysis (GSEA) exhibited a significant correlation between DD-iPSC marker expression and the existence of HERV-H LTR7s [enrichment score = 0.59, false-discovery rate (FDR)

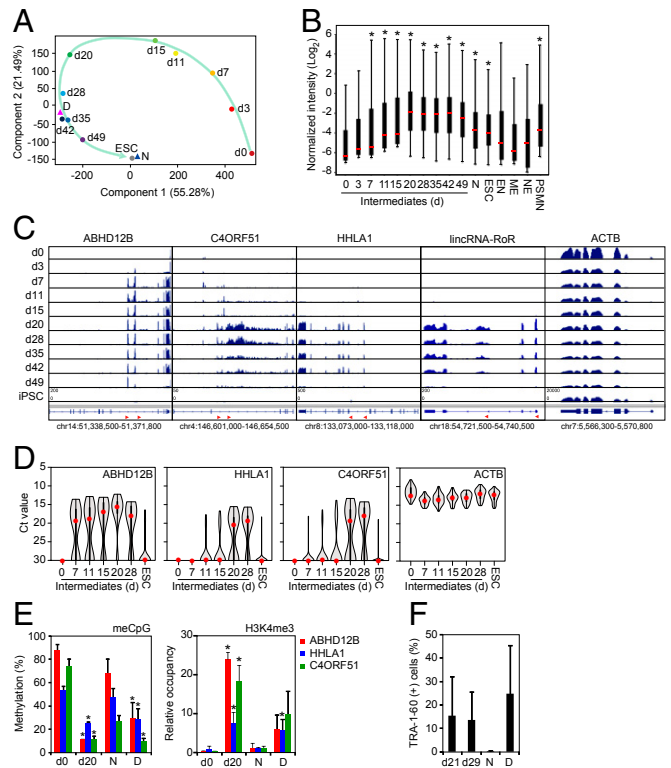


**Fig. 2.** Resemblance of DD-iPSC and partially reprogrammed cells. (A) Principal component analysis of DD-iPSC marker genes. Comparison of expression of 144 DD-iPSC marker genes in HDFs (day 0,  $n = 4$ ), intermediate reprogrammed cells derived from HDFs induced by OSKM [EGFP (+) cells on day 3 and TRA-1-60 (+) cells on d7-49,  $n = 3-4$  in each time point], ESCs ( $n = 4$ ), and normal (N,  $n = 18$ ) and DD (D,  $n = 37$ )-iPSC subclones. The green arrow indicates the route of reprogramming. (B) Distribution of DD-iPSC marker gene expression. The box plot shows expression of 144 DD-iPSC marker genes in microarray data and their distribution in intermediate reprogrammed cells [EGFP (+) cells on day 3 and TRA-1-60 (+) cells on days 7-49] and iPSCs were revealed by RNA-seq. Red arrowheads indicate the LTR7 position and direction in each locus. (C) Transcription of DD-iPSC markers from LTR7 during reprogramming. Expression of *ABHD12B*, *HHLA1*, *C4ORF51*, *lincRNA-RoR*, and *ACTB* in HDFs (day 0), intermediate reprogrammed cells [EGFP (+) cells on day 3 and TRA-1-60 (+) cells on days 7-49] and iPSCs were revealed by RNA-seq. Red arrowheads indicate the LTR7 position and direction in each locus. (D) All TRA-1-60 (+) cells transiently express DD-iPSC markers. Ct values plotted by single-cell qRT-PCR for *ABHD12B*, *HHLA1*, *C4ORF51*, and *ACTB* in intermediate reprogrammed cells (days 0-28 in the x axis) and ESCs. At least 42 single cells were analyzed for each sample. Red dots indicate median values. Gray hourglass shapes represent the distribution of Ct value. Ct 30 indicates undetectable expression, which was indicated by Ct values  $> 26$ . (E) Epigenetic statuses of LTR7s in TRA-1-60 (+) cells. The percentages of CpG methylation (Left) and H3K4me3 statuses (Right) in LTR7s on each locus including *ABHD12B*, *HHLA1*, and *C4ORF51* revealed by bisulfite conversion/pyrosequencing and ChIP-qPCR, respectively. Day 0, HDFs ( $n = 3$ ); day 20, TRA-1-60 (+) cells ( $n = 3$ ); N, normal iPSCs ( $n = 3$ ); D, DD-iPSCs ( $n = 3$ ). Error bars are SD.  $*P < 0.05$  vs. N was calculated by  $t$  test. (F) Neural differentiation-defective phenotype of TRA-1-60 (+) cells during reprogramming. Proportions of TRA-1-60 (+) cells after SFEBq neural inducing culture for 14 d.  $n = 3$ . Error bars are SDs.

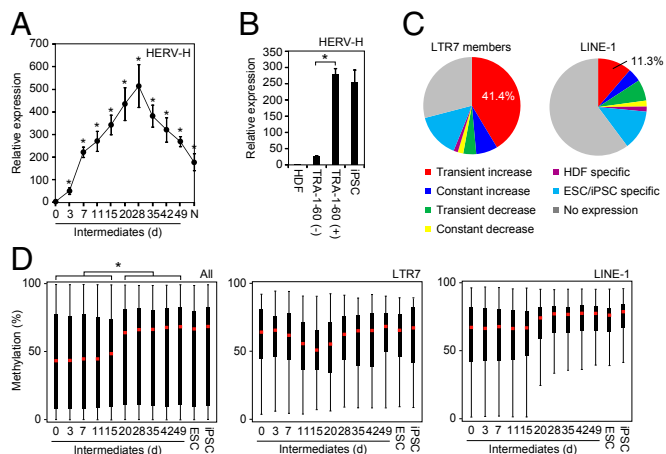


**Fig. 3.** Transient hyperactivation of LTR7s during iPSC generation. (A) Transition of total LTR7 transcription level during reprogramming. The plot shows the relative expression of total HERV-H in intermediate reprogrammed cells [EGFP (+) cells on day 3 and TRA-1-60 (+) cells on days 7–49] and normal iPSCs (N) compared with HDFs (day 0) revealed by qRT-PCR. Each value was normalized to that of *G3PDH*.  $n = 3$ . Error bars are SD.  $*P < 0.05$  vs. HDF was calculated by Dunnett test. (B) Abundant HERV-H expression in TRA-1-60 (+) intermediates. Shown are relative expression of HERV-H in HDFs, TRA-1-60 (–) or (+) cells on day 7 and normal iPSCs analyzed by qRT-PCR. Each value was normalized to that of *G3PDH*.  $n = 3$ . Error bars are SD.  $*P < 0.05$  was calculated by *t* test. (C) Expression patterns of the LTR7 family during reprogramming. Data are shown as LTR7 members and LINE-1 reads per kilobase of exon per million mapped reads (RPKM) in HDFs, TRA-1-60 (+) cells on day 20, and ESCs/normal iPSCs ( $n = 8$ ). (D) Distribution of CpG methylation during reprogramming. The box plots show the distribution of methylation level at CpGs on all probes (Left), LTR7 (Center), and LINE-1 (Right) regions with overhang sequences (250 bp) in HDFs (day 0), intermediate reprogrammed cells [EGFP (+) cells on d3 and TRA-1-60 (+) cells on days 7–49], ESCs, and normal iPSCs. Red and black bars indicate the median and quartile, respectively.  $n = 3$ . Post hoc pairwise comparisons were performed by Tukey's test ( $*P < 0.01$ ).

$q$ -value  $< 0.01$ ] (Fig. 1E), showing that aberrant activation of LTR7s is a characteristic feature of the DD phenotype.

**Similarity Between DD-iPSCs and Partially Reprogrammed Cells.** Next, we tried to understand why and how LTR7s were aberrantly activated in DD-iPSCs. To this end, we examined LTR7 activities during the course of iPSC generation. We sorted TRA-1-60–positive (+) reprogrammed cells on various days after retroviral transduction of OCT3/4, SOX2, KLF4, and myelocytomatosis oncogene (c-MYC) (subsequently referred to as OSKM) and analyzed their global gene expression by microarrays (11, 12). Using principle component analyses (PCA) with the 144 DD-iPSC markers, we found similarities between DD-iPSC subclones and TRA-1-60 (+) intermediate reprogrammed cells (Fig. 2A and Fig. S2). During reprogramming, TRA-1-60 (+) cells showed transiently enhanced expression of the DD-iPSC markers (including those driven by LTR7s), which reached significantly higher levels than in ESCs and normal iPSCs (Fig. 2B). When ESCs and normal iPSCs differentiated into endoderm (EN), mesoderm (ME), and neuroectoderm (NE), the expression of these markers significantly decreased. However, expression remained high in primitive streak-like mesendoderm (PSMN) (12). Deep sequencing of RNA (RNA-seq) from TRA-1-60 (+) cells exhibited the chimeric transcripts of *ABHD12B*, *HHLA1*, *C4ORF51*, and *lincRNA-RoR* with LTR7 sequences that meant transcription from intragenic LTR7s of HERV-Hs (Fig. 2C) (3, 10). Single-cell quantitative RT-PCR (qRT-PCR) showed that virtually all TRA-1-60 (+) cells—but not human dermal fibroblasts (HDFs) or ESCs—expressed the DD-iPSC marker genes related to

HERV-H LTR7s (Fig. 2D). Furthermore, in both TRA-1-60 (+) intermediate cells on day 20 and DD-iPSCs, we observed less CpG dinucleotide methylation and more trimethylation of lysine 4 on histone H3 (H3K4me3) in the LTR7-driven DD-iPSC marker genes (Fig. 2E). LTR7-driven DD-iPSC marker genes were highly expressed in TRA-1-60 (+) cells derived from HDFs as well as from adipose tissue-derived mesenchymal stem cells (mesoderm), astrocytes (ectoderm), and bronchial epithelium (endoderm) (Fig. S3). Furthermore, we found that on days 21 and 29, TRA-1-60 (+) cells showed defective neural differentiation, in that they still contained TRA-1-60 (+) cells even after in vitro directed neural differentiation (Fig. 2F). Overall, these data show that DD-iPSC clones are similar to TRA-1-60 (+) intermediate reprogrammed cells in both gene expression and neural differentiation ability.

**Genome-Wide LTR7 Activation During Reprogramming.** This last observation prompted us to examine the genome-wide LTR7 activity during reprogramming. qRT-PCR using a primer set for a conserved sequence of HERV-H LTR7 (13, 14) revealed that HERV-H transcripts transiently increased in TRA-1-60 (+) cells during reprogramming (Fig. 3A). The expression level of HERV-H in TRA-1-60 (+) intermediates on day 7 was significantly higher than those in TRA-1-60 (–) cells (Fig. 3B). RNA-seq showed that more than 40% of 3,771 LTR7 members in the human

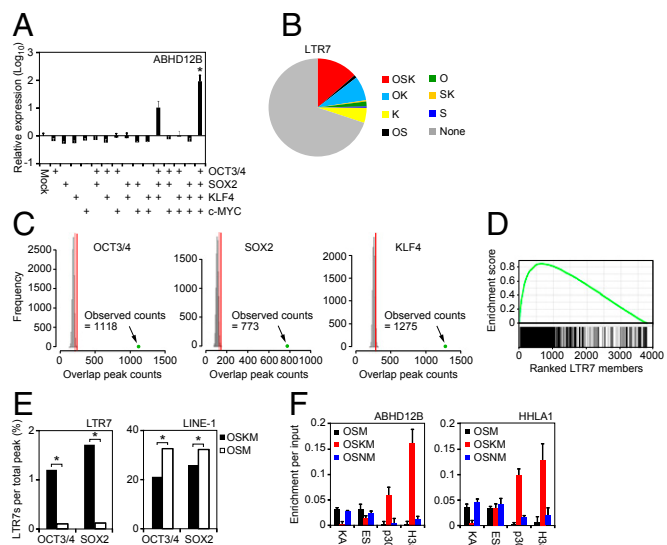


**Fig. 4.** Role of OSK in LTR7 activation. (A) OSK is required for activation of *ABHD12B* expression. Relative expression level of *ABHD12B* on day 7 post-transduction for all combinations of OSKM. Error bars are SDs.  $n = 3$ .  $*P < 0.05$  vs. Mock was calculated by Dunnett test. (B) Distribution of reprogramming factor occupancy on all LTR7s loci revealed by ChIP-seq. (C) Significance of the interaction of reprogramming factors to LTR7s. Histograms show counts of peaks for OCT3/4, SOX2, or KLF4 overlapped with randomly selected regions (10,000 random trials). The 95th percentile count of distribution is marked by red lines. Green dots show counts of ChIP-seq peaks on LTR7 regions with overhang sequences (250 bp). (D) GSEA plot showing enrichment of OSK occupancies in expressed LTR7s. Expressed LTR7 family members in TRA-1-60 (+) cells on day 15 are enriched in the set of LTR7s that show full-array OSK binding ( $P = 2.4e-155$ ). (E) KLF4-dependent binding of OCT3/4 and SOX2 to LTR7s. Bars show the percentage of OCT3/4- or SOX2-bound LTR7 family members and LINE-1 in HDFs transduced with OSKM (closed) or OSM (open) on day 3 posttransduction.  $\chi^2$  tests were performed between the proportions ( $*P < 0.05$ ). (F) Interaction between HERV-H loci and chromatin modifiers. ChIP assays were performed to analyze the interaction of *ABHD12B* and *HHLA1* loci with KAP-1, ESET, p300, and pan-acetyl histone H3 (H3ac) occupancy in HDFs transduced with OSM, OSKM, or OSNM on day 3 were analyzed by ChIP-qPCR.  $n = 3$ . Error bars are SD.

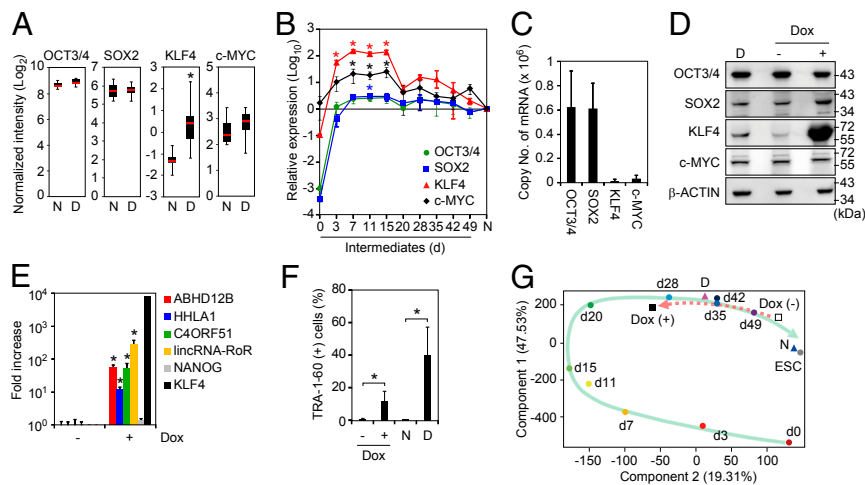


**Fig. 5.** Role of KLF4 in the DD phenotype. (A) High expression of KLF4 in DD-iPSCs. Expression levels of total *OCT3/4*, *SOX2*, *KLF4*, and *c-MYC* in normal- (N;  $n = 18$ ) and DD- (D;  $n = 37$ ) iPSC primary subclones in microarray analysis. \*FDR < 0.05 vs. N was calculated by *t* test. (B) Relative expression of total OSKM in intermediate reprogrammed cells were quantified by qRT-PCR and compared with those in iPSC. Each value was normalized to that of *G3PDH*.  $n = 3$ . Error bars are SDs. \* $P < 0.05$  vs. iPSC (N) was calculated by Dunnett test. (C) Copy number of OSKM mRNAs in iPSCs. Data are shown as copy numbers of mRNA per 50 ng of total RNA calculated using a plasmid encoding each factor as a standard in qRT-PCR.  $n = 23$ . Error bars are SDs. (D) Expression of KLF4 protein. Western blot analyses of expression of *OCT3/4*, *SOX2*, *KLF4*, *c-MYC*, and  $\beta$ -ACTIN proteins in DD-iPSCs (D) and normal iPSCs (N) transduced with Dox-inducible KLF4 maintained with (+) or without (-) Dox. (E) KLF4 induces DD-iPSC marker expression in iPSCs. Bars show the relative expression levels of *ABHD12B*, *HHLA1*, *C4ORF51*, *lincRNA-RoR*, *NANOG*, and *KLF4* in KLF4-overexpressing iPSCs analyzed by qRT-PCR. Each value was normalized to that of *G3PDH*.  $n = 3$ . Error bars are SDs. \* $P < 0.05$  vs. Dox (-) were calculated by *t* test. (F) KLF4 prevents neural differentiation. Normal iPSCs transduced with Dox-inducible KLF4 were differentiated into neural cells using the SFEBq method with (+) or without (-) Dox. Bars show the percentages of TRA-1-60 (+) cells after a SFEBq neural inducing culture for 14 d. N and D represent normal and DD-iPSCs, respectively.  $n = 3$ . Error bars are SDs. \* $P < 0.05$  was calculated by *t* test. (G) KLF4 changes the fate of iPSCs. PCA of microarray data from HDFs (day 0), TRA-1-60 (+) intermediate reprogrammed cells, normal iPSC subclones (N), DD-iPSC subclones (D), and Dox-inducible KLF4-transduced iPSCs with (+) or without (-) Dox for the 144 DD-iPSC marker genes. The green arrow indicates the route of reprogramming. The red broken arrow indicates the fate transition after induction of the KLF4 transgene.

genome were transiently activated in TRA-1-60 (+) intermediate reprogrammed cells (Fig. 3C), whereas another transposable element, long-interspersed element-1 (LINE-1), showed varying expression patterns. Array-based analyses revealed that CpG methylation of LTR7 regions in TRA-1-60 (+) cells transiently decreased (Fig. 3D) (15). In contrast, global CpGs and those around LINE-1 elements gradually became methylated during reprogramming. Therefore, LTR7s were activated in a genome-wide manner during OSKM-mediated reprogramming.

**Role of OSK in LTR7 Activation.** We next examined how OSKM helps activate the LTR7s during reprogramming. In day 7-transduced HDFs, we found that forced expression of OSK or OSKM, but not any single reprogramming factor or another combination, induced expression of the LTR7-driven gene *ABHD12B* (Fig. 4A). Thus, *OCT3/4*, *SOX2*, and *KLF4* are all required for LTR7 activation. ChIP and sequencing (ChIP-seq) analyses showed that ~15% of 3,771 LTR7s had cobinding of *OCT3/4*, *SOX2*, and *KLF4* (OSK), ~8% had cobinding of *OCT3/4* and *KLF4* (OK), and ~5% had binding of *KLF4* alone (K) (Fig. 4B). Compared with random binding, the concentrations of *OCT3/4*, *SOX2*, or *KLF4* binding in LTR7s was highly significant (Fig. 4C). In addition, GSEA exhibited a significant correlation between OSK binding and HERV-H LTR7 expression in TRA-1-60 (+) cells (enrichment score = 0.85,  $P = 2.4 \times 10^{-155}$ ) (Fig. 4D). The number of *OCT3/4*- and *SOX2*-bound LTR7s markedly decreased in the absence of *KLF4* ( $P = 2.2 \times 10^{-16}$  for both *OCT3/4* and *SOX2*) (Fig. 4E), but such drastic decreases were not observed in *OCT3/4*- or *SOX2*-binding to LINE-1. Two proteins, KAP-1 (KRAB-associated protein 1) and histone methyltransferase SET domain bifurcated 1 (ESET), have been shown to be critical in suppression of endogenous retroviruses (16). ChIP experiments revealed that in HDFs transduced with OSKM, the binding of KAP-1 to LTR7s significantly decreased in *ABHD12B* and *HHLA1* loci, but this

decrease was not observed with OSM or OSNM (OSM with *NANOG* instead of *KLF4*) (Fig. 4F). In addition, the interaction between p300 and acetylated histone H3 was enriched by OSKM transduction, but not when *KLF4* was absent (Fig. 4F). Therefore, *KLF4* activates LTR7s by promoting OSK binding, recruiting the coactivator p300, and excluding KAP-1.

**KLF4, a DD-iPSC Marker, Activates LTR7.** In addition to LTR7-driven transcripts, we identified *KLF4* as a marker gene associated with the DD phenotype (Fig. 1D). Among the OSKM reprogramming factors, only *KLF4* was enriched in DD-iPSC subclones (Fig. 5A). Whether *KLF4* expression was derived from transgene or endogenous locus differed among clones (Fig. S4A). In the subclones derived from TIG118-4F1 and 451F3, the expression of endogenous *KLF4* highly correlated to the DD phenotype (Fig. S4B). On the other hand, there was no significant correlation between neural differentiation potentials and endogenous *KLF4* expression in the subclones derived from TIG108-4F3 and TKCBV5-6, which mainly expressed exogenous *KLF4* (Fig. S4B). These data suggest that *KLF4* expression including both aberrant activation of endogenous genes and insufficient silencing of retroviral vectors could be associated with the DD phenotype. We therefore analyzed the expression of *KLF4*, together with the remaining reprogramming factors, during iPSC generation. Total expression levels of *OCT3/4* and *SOX2* (from both endogenous genes and transgenes) increased more than 1,000-fold within 3 d after retroviral transduction and approached the levels in ESCs/iPSCs (Fig. 5B). After retroviral transgenes were silenced, the expression of *OCT3/4* and *SOX2* remained high because the endogenous genes were induced. Conversely, overexpression of *KLF4* was transient and decreased once the retroviral transgenes were silenced (Fig. 5A and B). Accordingly, the copy number of *KLF4* mRNA was less than 1/40 of those for *OCT3/4* and *SOX2* in ESCs and normal iPSCs (Fig. 5C). This

fact develops the transient increase of KLF4 expression during reprogramming toward iPSCs. On the other hand, the expression of OCT3/4 and SOX2 are constant even after transgene silencing occurred between days 15 and 20 posttransduction. Overall, increased expression of *KLF4* correlated with aberrant activation of LTR7s in both the reprogramming process and in DD-iPSCs.

To further examine the role of KLF4 in LTR7 activation, we introduced a doxycycline (Dox)-inducible KLF4 expression cassette into normal iPSCs using a PiggyBac transposon system (17) (Fig. 5D). Dox-induced KLF4 expression activated the LTR7-related transcripts *ABHD12B*, *HHLA1*, *C4ORF51*, and *lincRNA-RoR* but did not affect non-LTR-related genes, such as *NANOG* (Fig. 5E). Furthermore, overexpression of KLF4 in normal iPSCs produced the DD phenotype (Fig. 5F) (18). In contrast to neural lineage commitment, we observed no effects of KLF4 on the differentiation potentials of iPSCs into EN, ME, and PSMN (Fig. S5). This tendency was common between DD-iPSCs and KLF4-overexpressing iPSCs. PCA on the 144 DD-iPSC markers showed that KLF4-overexpressing iPSCs are quite similar to TRA-1-60 (+) intermediate reprogrammed cells (Fig. 5G), which confirms that KLF4 helps establish the DD phenotype.

To clarify the specificity by which KLF4 activates HERV-Hs in HDFs, we replaced KLF4 in the OSKM induction mixture with the reprogramming factor NANOG (referred to as OSNM). OSNM induced a few TRA1-60 (+) cells and ESC-like colonies on day 28 (Fig. S6A). In TRA-1-60 (+) cells induced by OSNM, the expressions of KLF4 (Fig. S6B), HERV-Hs (Fig. S6C), and LTR7-driven genes (Fig. S6D) were only slightly activated. Therefore, overexpression of KLF4 and hyperactivation of HERV-H LTR7s are strongly correlated with efficient reprogramming in iPSC generation.

We next performed loss-of-function experiments to further investigate the roles of KLF4 and LTR7 in reprogramming and the DD phenotype. We designed four sets of short hairpin RNAs (shRNAs): one targeted *KLF4* (shKLF4); two targeted LTR7 sequences conserved among *ABHD12B*, *HHLA1*, *C4ORF51*, and *lincRNA-RoR* (shLTR7-1 and shLTR7-2); and one targeted *lincRNA-RoR* (shRoR). In DD-iPSCs, shKLF4 and shLTR7-1, but not shRoR, significantly suppressed the total expression of HERV-Hs (Fig. 6A). The two shRNAs targeting the conserved LTR7 sequences effectively suppressed *ABHD12B*, *HHLA1*, *C4ORF51*, and *lincRNA-RoR*, but did not suppress *NANOG* (Fig. 6B). shRoR specifically repressed *lincRNA-RoR* expression but did not affect *ABHD12B*, *HHLA1*, *C4ORF51*, or *NANOG* (Fig. 6B). Suppressing KLF4 or HERV-H LTR7s in DD-iPSCs effectively reversed the DD phenotype and made the cells comparable to normal iPSCs (Fig. 6C). We observed a similar trend for shRoR, but the change was not statistically significant ( $P = 0.09$ ). In addition, shLTR7-1 canceled the DD phenotype of KLF4-overexpressing iPSCs (Fig. 6D). Transducing these shRNAs with OSKM reduced the number of TRA-1-60 (+) cells on days 7 and 11 (Fig. 6E) and almost completely inhibited the generation of iPSC colonies (Fig. 6F). These data confirmed the important roles of KLF4 and LTR7 in reprogramming and the DD phenotype.

## Discussion

In this study, we found that genome-wide HERV-Hs, including *lincRNA-RoR*, are transiently hyperactivated during reprogramming toward iPSCs and play important roles in this process. However, when reprogramming is complete and cells acquire full pluripotency, HERV-H LTR7 activity should decrease to levels comparable with those in ESCs. Failure to resile this activity leads to the DD phenotype. This observation resembles NANOG, which promotes induction and maintenance of pluripotency, but suppress differentiation when aberrantly expressed (19). We also found that during reprogramming, OSK factors bind to and activate LTR7s. Therefore, a major mechanism by which OSK reprogramming factors promote human iPSC generation is by

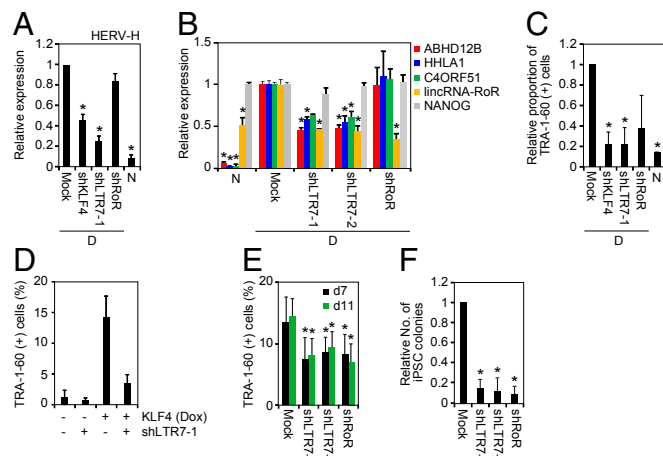


Fig. 6. Loss of function experiments to test roles of KLF4 and LTR7s in reprogramming and the DD phenotype. (A) KLF4 is responsible for HERV-H expression. Shown are relative expressions of HERV-H in DD-iPSCs (D) transduced with *KLF4* shRNA (shKLF4), LTR7 shRNA-1 (shLTR7-1), or shRoR, and normal iPSCs (N) compared with those of Mock-transduced DD-iPSCs. Each value was normalized to that of *G3PDH*.  $n = 3$ . Error bars are SDs.  $n = 3$ .  $*P < 0.05$  vs. Mock was calculated by Dunnett test. (B) Knockdown of LTR7 expression. Bars show relative expression of *ABHD12B*, *HHLA1*, *C4ORF51*, *lincRNA-RoR*, and *NANOG* in normal iPSCs (N) and DD-iPSCs (D) transduced with empty vector (Mock), LTR7 shRNA-encoding vectors (shLTR7-1 and -2), or shRoR compared with Mock analyzed by microarray. Error bars are SDs.  $n = 2$ .  $*P < 0.05$  vs. Mock was calculated by Dunnett test. (C) Suppression of KLF4/HERV-H LTR7 rescues the DD phenotype. Shown are the relative proportions of residual TRA-1-60 (+) cells on day 14 after neural differentiation of DD-iPSCs (D) carrying empty vector (Mock), LTR7 shRNAs (shLTR7-1), or shRoR, compared with normal iPSCs (N).  $n = 3$ .  $*P < 0.05$  vs. Mock was calculated by Dunnett test. (D) Suppression of LTR7 rescues the KLF4-induced DD phenotype. Shown are the percentages of residual TRA-1-60 (+) cells on day 14 after neural differentiation of normal iPSCs carrying dox-inducible KLF4, and empty vector or LTR7 shRNA (shLTR7-1). Differentiation was performed in the presence (+) or absence (-) of Dox. Error bars are SDs.  $n = 2$ . (E) LTR7 activity enhances reprogramming efficiency. Shown are the percentages of TRA-1-60 (+) cells on days 7 (black) and 11 (green) posttransduction of OSKM with empty vector (Mock), LTR7 shRNA-encoding vectors (shLTR7-1 and -2), or shRoR vector.  $n = 3$ . Error bars are SDs.  $*P < 0.05$  vs. Mock was calculated by Dunnett test. (F) LTR7 activity facilitates iPSC generation. Shown are the relative numbers of iPSC colonies on day 25 posttransduction of OSKM with empty vector (Mock), LTR7 shRNA-encoding vectors (shLTR7-1 and -2), or shRoR vector. Error bars are SDs.  $n = 4$ .  $*P < 0.05$  vs. Mock was calculated by Dunnett test.

transiently hyperactivating HERV-H LTR7s. Noteworthy, our findings suggest the significance of the transition state of intermediate reprogrammed cells, including hyperactivation of HERV-Hs induced by reprogramming factors. Among these cells, KLF4 particularly plays important roles for the activation of HERV-Hs. Our data also revealed that NANOG as a replacer of KLF4 in iPSC generation can induce less HERV-H activity during reprogramming (11). Therefore, the reason why the significant difference of reprogramming activity between KLF4 and NANOG can be explained with our data.

Recent study by Lu et al. showed that HERV-H activity regulated by OCT3/4 and p300 is important for generation and self-renewal of iPSCs (20). Among OSKM reprogramming factors, we showed that KLF4 levels are the most important for activating and resuppressing LTR7s. First, the binding of OCT3/4 and SOX2 to LTR7s was highly dependent on the presence of KLF4. Corroborating this finding, we and others have previously demonstrated that the KLF4 protein binds to OCT3/4 and SOX2 proteins. Second, we detected a surge in KLF4 expression during reprogramming, which was correlated with the transient hyperactivation of LTR7s. At around 15 d after transduction, overexpression of

12430 | www.pnas.org/cgi/doi/10.1073/pnas.1413299111

Ohnuki et al.

OSKM from retroviral transgenes is silenced. However, OCT3/4 and SOX2 maintained high expression levels because of the activation of their endogenous genes. In contrast, the endogenous KLF4 gene was only weakly activated, thus its total expression level rapidly decreased. In DD-iPSC clones and subclones, KLF4 is expressed at higher levels than in normal iPSCs, in agreement with the expression level of KLF4 helping determine LTR7 activity. Furthermore, we found that KLF4, together with OCT3/4 and SOX2, increased the binding of coactivator p300 to LTR7s and decreased KAP-1 binding to LTR7s. It has been shown that both KLF4 and KAP-1 bind to methylated DNA (21), suggesting a competition between the two proteins. Overall, we found that KLF4 strongly promotes LTR7 activity.

Among LTR7-driven transcripts, we found that *lincRNA-RoR* importantly influenced reprogramming and the DD phenotype. This result is consistent with a report from Loewer et al., who showed that *lincRNA-RoR* promoted iPSC generation (22). The authors identified *lincRNA-RoR* as one of 10 lincRNAs whose expression levels were higher in iPSCs than in ESCs (22). In contrast, the levels of *lincRNA-RoR* within most iPSC clones in our study were comparable to those of ESCs. Only DD-iPSCs showed higher expression levels. The functions of *lincRNA-RoR* remain elusive, but it may serve as a microRNA (miRNA) sponge that protects SOX2 and NANOG from miRNA-mediated degradation by sharing the binding sites of miRNAs that suppress the core transcription factors (23). Alternatively, *lincRNA-RoR* may suppress p53 (24), which inhibits reprogramming (25–29). Other LTR7-driven transcripts besides *lincRNA-RoR* likely also contribute to reprogramming and the DD phenotype, given that shRoR only weakly reversed the DD phenotype compared with shKLF4 or shLTR7s. Further studies, including genetic deletion of *lincRNA-RoR*, are required to fully understand how the activation of LTR7s contributes to reprogramming and the DD phenotype.

Our results suggest that reprogramming processes may use unique transposable elements in each species. Because neither HERV-H sequences nor *lincRNA-RoR* are conserved in mice, their activation cannot contribute to mouse reprogramming. Bourque and colleagues compared the binding sites of OCT3/4

and NANOG in their target genes and showed that species-specific transposable elements have substantially altered the transcriptional circuitry of pluripotent stem cells (6). Thus, ERV-1, including HERV-H, plays a major role in reprogramming human cells, whereas ERV-K, which is enriched in Oct3/4- and Nanog-binding sites in mice (6), may be involved in reprogramming mouse cells. Another study showed that a small portion of mouse ESCs and iPSCs express ERV-L retroviruses and possess the ability to differentiate not only into embryonic lineages but also into extraembryonic cells (30). Recently, Friedli et al. showed that aberrant activation of intracisternal A particle, a member of ERV-K, occurred during reprogramming of mouse embryonic fibroblasts toward iPSCs, as well as HERV-H behavior in a human case, which may suggest the importance of ERV activity in reprogramming beyond species (31). An important future task will involve examining the roles of species-specific ERVs in reprogramming and pluripotency.

## Materials and Methods

Detailed descriptions of materials and methods are available in *SI Materials and Methods*. See *Dataset S3* for primer sequences used in this study. Plasmids are available from Addgene ([www.addgene.org](http://www.addgene.org)).

**ACKNOWLEDGMENTS.** We thank D. Srivastava for critical reading of the manuscript; G. Howard for editorial assistance; S. Arai, S. Ando, Y. Inoue, and N. Amano for technical assistance; M. Koyanagi-Aoi for sharing data; A. Morizane and J. Takahashi for guidance regarding the cellular differentiation; and H. Suemori, T. Kitamura, K. Okita, K. Eto, N. Takayama, and K. Woltjen for providing important materials. We are also grateful to Y. Miyake, R. Kato, E. Minamitani, S. Takeshima, R. Fujiwara, Y. Higuchi and K. Nakahara for administrative support. This work was supported in part by Grants-in-Aid for Scientific Research from the Japanese Society for the Promotion of Science (JSPS) and from the Ministry of Education, Culture, Sports, Science, and Technology (MEXT); a grant from the Leading Project of the MEXT; a grant from the Funding Program for World-Leading Innovative Research and Development in Science and Technology (First Program) of the JSPS; a grant from Core Center for iPSC Cell Research, Research Center Network for Realization of Regenerative Medicine; a grant from World Premier International Research Center Initiative (WPI), MEXT; a grant from Japan Foundation for Applied Enzymology; and iPSC Cell Research Fund. M.O. was supported as a JSPS fellow.

- Thomson JA, et al. (1998) Embryonic stem cell lines derived from human blastocysts. *Science* 282(5391):1145–1147.
- Takahashi K, et al. (2007) Induction of pluripotent stem cells from adult human fibroblasts by defined factors. *Cell* 131(5):861–872.
- Koyanagi-Aoi M, et al. (2013) Differentiation-defective phenotypes revealed by large-scale analyses of human pluripotent stem cells. *Proc Natl Acad Sci USA* 110(51):20569–20574.
- Lander ES, et al.; International Human Genome Sequencing Consortium (2001) Initial sequencing and analysis of the human genome. *Nature* 409(6822):860–921.
- Santoni FA, Guerra J, Luban J (2012) HERV-H RNA is abundant in human embryonic stem cells and a precise marker for pluripotency. *Retrovirology* 9:111.
- Kunaro G, et al. (2010) Transposable elements have rewired the core regulatory network of human embryonic stem cells. *Nat Genet* 42(7):631–634.
- Takayama N, et al. (2010) Transient activation of c-MYC expression is critical for efficient platelet generation from human induced pluripotent stem cells. *J Exp Med* 207(13):2817–2830.
- Okita K, et al. (2011) A more efficient method to generate integration-free human iPSC cells. *Nat Methods* 8(5):409–412.
- Morizane A, Doi D, Kikuchi T, Nishimura K, Takahashi J (2011) Small-molecule inhibitors of bone morphogenic protein and activin/nodal signals promote highly efficient neural induction from human pluripotent stem cells. *J Neurosci Res* 89(2):117–126.
- Kelley D, Rinn J (2012) Transposable elements reveal a stem cell-specific class of long noncoding RNAs. *Genome Biol* 13(11):R107.
- Tanabe K, Nakamura M, Narita M, Takahashi K, Yamanaka S (2013) Maturation, not initiation, is the major roadblock during reprogramming toward pluripotency from human fibroblasts. *Proc Natl Acad Sci USA* 110(30):12172–12179.
- Takahashi K, et al. (2014) Induction of pluripotency in human somatic cells via a transient state resembling primitive streak-like mesendoderm. *Nat Commun* 5:3678.
- Jern P, Sperber GO, Ahlsén G, Blomberg J (2005) Sequence variability, gene structure, and expression of full-length human endogenous retrovirus H. *J Virol* 79(10):6325–6337.
- Liang Q, Xu Z, Xu R, Wu L, Zheng S (2012) Expression patterns of non-coding spliced transcripts from human endogenous retrovirus HERV-H elements in colon cancer. *PLoS ONE* 7(1):e29950.
- Lister R, et al. (2011) Hotspots of aberrant epigenomic reprogramming in human induced pluripotent stem cells. *Nature* 471(7336):68–73.
- Rowe HM, et al. (2013) De novo DNA methylation of endogenous retroviruses is shaped by KRAB-ZFPs/KAP1 and ESET. *Development* 140(3):519–529.
- Woltjen K, et al. (2009) piggyBac transposition reprograms fibroblasts to induced pluripotent stem cells. *Nature* 458(7239):766–770.
- Kim H, et al. (2011) miR-371-3 expression predicts neural differentiation propensity in human pluripotent stem cells. *Cell Stem Cell* 8(6):695–706.
- Darr H, Mayshar Y, Benvenisty N (2006) Overexpression of NANOG in human ES cells enables feeder-free growth while inducing primitive ectoderm features. *Development* 133(6):1193–1201.
- Lu X, et al. (2014) The retrovirus HERVH is a long noncoding RNA required for human embryonic stem cell identity. *Nat Struct Mol Biol* 21(4):423–425.
- Quenneville S, et al. (2011) In embryonic stem cells, ZFP57/KAP1 recognize a methylated hexanucleotide to affect chromatin and DNA methylation of imprinting control regions. *Mol Cell* 44(3):361–372.
- Loewer S, et al. (2010) Large intergenic non-coding RNA-RoR modulates reprogramming of human induced pluripotent stem cells. *Nat Genet* 42(12):1113–1117.
- Wang Y, et al. (2013) Endogenous miRNA sponge lincRNA-RoR regulates Oct4, Nanog, and Sox2 in human embryonic stem cell self-renewal. *Dev Cell* 25(1):69–80.
- Zhang A, et al. (2013) The human long non-coding RNA-RoR is a p53 repressor in response to DNA damage. *Cell Res* 23(3):340–350.
- Kawamura T, et al. (2009) Linking the p53 tumour suppressor pathway to somatic cell reprogramming. *Nature* 460(7259):1140–1144.
- Hong H, et al. (2009) Suppression of induced pluripotent stem cell generation by the p53-p21 pathway. *Nature* 460(7259):1132–1135.
- Banito A, et al. (2009) Senescence impairs successful reprogramming to pluripotent stem cells. *Genes Dev* 23(18):2134–2139.
- Utikal J, et al. (2009) Immortalization eliminates a roadblock during cellular reprogramming into iPSCs. *Nature* 460(7259):1145–1148.
- Marion RM, et al. (2009) A p53-mediated DNA damage response limits reprogramming to ensure iPSC cell genomic integrity. *Nature* 460(7259):1149–1153.
- Macfarlan TS, et al. (2012) Embryonic stem cell potency fluctuates with endogenous retrovirus activity. *Nature* 487(7405):57–63.
- Friedli M, et al. (2014) Loss of transcriptional control over endogenous retroelements during reprogramming to pluripotency. *Genome Res*.

# Supporting Information

Ohnuki et al. 10.1073/pnas.1413299111

## SI Materials and Methods

**Cell Culture.** Human dermal fibroblasts (HDFs) obtained from the Japanese Collection of Research Bioresources were maintained in DMEM (Nacalai tesque) containing 10% FBS (Japan Bioserum) and 0.5% penicillin and streptomycin (Pen/Strep, Life Technologies). PLAT-E (1) and PLAT-GP cells were maintained in the same medium. Embryonic stem cell (ESC) clones obtained from WiCELL (H1 and H9) (2) and Kyoto University (KhES1 and KhES3) (3) were maintained in Primate ESC medium (ReproCELL) supplemented with 4 ng/mL recombinant human basic fibroblast growth factor (bFGF, Wako) and 0.5% Pen/Strep on mitomycin C (MMC)-treated SNL feeder cells, or in mTeSR1 (Veritas) on Matrigel-coated plates (growth factor reduced; BD Biosciences) (4).

**Reprogramming.** Reprogramming experiments were conducted as described previously (4, 5). To generate retrovirus, we introduced retroviral plasmids into PLAT-E or PLAT-GP cells using the FuGENE 6 transfection reagent (Promega) (1). On the following day, the medium was replaced with an equal volume of fresh medium and cells were incubated overnight. The virus-containing supernatant was collected, filtered through a 0.45- $\mu$ m pore-size cellulose acetate filter (Whatman) to remove cell debris, and supplemented with 4  $\mu$ g/mL Polybrene (Nacalai tesque). Appropriate combinations of viruses were mixed and exposed to HDFs expressing the mouse *Slc7a1* gene overnight. This point was designated as day 0. To collect the samples on day 3 posttransduction, we introduced pMXs-internal ribosome entry site-EGFP (IG) encoding SOX2 instead of pMXs-SOX2, along with OKM (OCT3/4, KLF4, and c-MYC), and sorted EGFP (+) cells by flow cytometry. TRA-1-60 (+) intermediate reprogrammed cells were collected by magnetic activated cell sorting as described previously. For reprogramming experiments with shRNA transduction, 1  $\mu$ g/mL puromycin was added to the medium from days 3–7 to eliminate untransduced cells. Cells were harvested on day 7 and reseeded onto MMC-inactivated SNL feeders to generate induced pluripotent stem cells (iPSCs). On the following day, the medium was replaced with Primate ESC medium supplemented with 4 ng/mL bFGF, and the medium was then changed every other day. The number of iPSC colonies was counted on day 25. We distinguished bona fide iPSC colonies from non-iPSC colonies based on their morphological differences (4).

**Neural Differentiation and Flow Cytometry.** The single-cell suspensions of pluripotent stem cells were prepared using CTX solution and AccuMAX (Innovative Cell Technology), and then transferred at  $9 \times 10^3$  cells per well of Lipidure-coated low-binding 96-well plates (NOF Corporation) in 8GMK medium consisting of Glasgow modified eagle medium (Life Technologies), 8% knockout serum replacement (Life Technologies), 1% nonessential amino acids (NEAA; Life Technologies), 1% sodium pyruvate (Sigma), and 100 nM 2-mercaptoethanol (2-ME, Life Technologies) supplemented with 500 nM A-83-01 (Stemgent) and 100 nM LDN193189 (Stemgent). The medium was carefully half-changed on days 5, 8, and 11. On day 14, the aggregates were collected to a 1.5-mL tube and pelleted by centrifugation at  $200 \times g$  for 5 min. The pellet was washed with PBS and then dispersed to single cells using AccuMAX, and then cells were used for immunostaining. We used propidium iodide (Life Technologies) or DAPI (Life Technologies) to distinguish dead cells. Samples were analyzed using a FACS Aria II (Becton Dickinson).

**Primitive Streak-Like Mesendoderm Differentiation.** Primitive streak-like mesendoderm differentiation was performed as described previously (6, 7). In brief, single-cell suspensions of human iPSCs were plated onto fibronectin-coated plates (BD Biosciences) in DMEM/F12 (Life Technologies) supplemented with 1% Insulin-Transferrin-Selenite (Life Technologies), 1% Glutamax (Life Technologies), 1% NEAA, 2% B27 (Life Technologies), 100 nM 2-ME, and 0.5% Pen/Strep. We added 3  $\mu$ M CHIR99021 (Stemgent) and 50 ng/mL Activin A (Peprotech) on day 1, 3  $\mu$ M CHIR99021, 25 ng/mL Activin A and 20 ng/mL bFGF on day 2 and 3  $\mu$ M CHIR99021, 10 ng/mL Activin A, 20 ng/mL bFGF and 40 ng/mL BMP4 (R&D Systems) on day 3.

**Endoderm Differentiation.** Endoderm differentiation was performed as described previously, with slight modification (6, 8). The single-cell suspensions of human pluripotent stem cells were plated onto Matrigel-coated plates in RPMI1640 (Life Technologies) containing 2% B27, 100 ng/mL Activin A, 3  $\mu$ M CHIR99021, and 0.5% Pen/Strep. We added 0.5 mM sodium butyrate (Sigma) on days 1–3, and then carried out sodium butyrate-free culture until day 7.

**Mesoderm Differentiation.** The mesodermal differentiation was performed as described previously, with slight modification (6, 9). The single-cell suspensions of human pluripotent stem cells were plated onto collagen I-coated plates (BD Biosciences) in DMEM/F12 containing 2% B27, 100 ng/mL Activin A, 3  $\mu$ M CHIR99021 and 0.5% Pen/Strep. Forty-eight hours later, the medium was replaced with DMEM/F12 supplemented with 2% B27, 25 ng/mL BMP4, and 0.5% Pen/Strep. The medium was changed every other day until day 8.

**Antibodies.** The following antibodies were used in the study: Alexa 488-conjugated TRA-1-60 (1:20, 560173, BD Biosciences), anti-polysialylated neuronal cell-adhesion molecule (PSA-NCAM) antibody (1:50; MAB5324, Millipore), APC-labeled anti-C-X-C chemokine receptor type 4 (CXCR4) (1:5; FAB170A, R&D Systems), phycoerythrin (PE)-labeled antiplatelet-derived growth factor receptor- $\alpha$  (PDGFRA) (1:5; 556002, BD Pharmingen), APC-conjugated anti-BRACHYURY (1:5; IC20851A, R&D Systems), Alexa 647-conjugated anti-mouse IgM antibody (1:500; A-21238, Life Technologies), PE-conjugated TRA-1-60 (1:5; 560193, BD Pharmingen), and anti-PE microbeads (130-048-801, Miltenyi Biotec). For Western blot analyses, we used anti-OCT3/4 (1:600; sc-5279, Santa Cruz Biotechnology), anti-SOX2 (1:1,000; ab97959, Abcam), anti-KLF4 (1:500; AF3640, R&D Systems), anti-c-MYC (1:200; sc-42, Santa Cruz), anti- $\beta$ -actin (1: 5,000; A5441, Sigma), anti-mouse IgG HRP (1:3,000; 7076S, Cell Signaling Technology), anti-rabbit IgG-HRP (1:2,000; 7074S, Cell Signaling), and anti-goat IgG-HRP (1:2,000; sc-2056, Santa Cruz). For ChIP analyses, we used anti-Flag M2 (F1804, Sigma), antitrifluoromethylated lysine 4 of histone H3 antibody (MAB10304, Wako), anti-p300 (sc-585, Santa Cruz), anti-KAP1 (ab10483, Abcam), anti-SET domain bifurcated 1 (sc-66884, Santa Cruz), and antihistone H3Ac (pan acethyl) (39139, Active Motif).

**Quantitative RT-PCR.** Total RNA was isolated using the Qiazol reagent (Qiagen) and a miRNeasy mini kit (Qiagen). CDNA was generated with a ReverTra Ace- $\alpha$  kit (Toyobo) and oligo dT<sub>20</sub> primer. For quantitative RT-PCR (qRT-PCR), reaction mixtures were set up in triplicate using SYBR premix Ex-Taq II (Takara) and run using a StepOne instrument (Applied Biosciences). The levels of mRNA were normalized to *G3PDH* expression, and

then relative expression was calculated as the fold-change from the control. Primer sequences for each gene are shown in [Dataset S3](#).

**Gene-Expression Analysis by Microarray.** Total RNA was purified as described above and the quality was evaluated using a 2100 Bioanalyzer (Agilent Technologies). Total RNA (50 ng) was labeled with cyanine 3-CTP and used for hybridization with a SurePrint G3 Human GE 8 × 60 K array (G4851A, Agilent Technologies) with a one-color protocol. Hybridized arrays were scanned with a Microarray Scanner System (G2565BA, Agilent Technologies), and extracted signals were analyzed using GeneSpring v12.6 software (Agilent Technologies). Gene-expression values were normalized by 75th percentile shifts. Differentially expressed genes between normal and differentiation-defective (DD)-iPSCs were extracted by comparison using *t* tests with Benjamini and Hochberg corrections [ $FC > 2.0$ , false-discovery rate (FDR)  $< 0.05$ ].

**CpG Methylation Analysis by Microarray.** Genomic DNA was extracted using a DNeasy Blood and Tissue Kit (Qiagen). Purified genomic DNA (30 ng) was used for bisulfite CT conversion with an EZ DNA methylation kit (Zymo Research). Bisulfite-treated DNA was whole-genome amplified and hybridized to Human-Methylation450 BeadChip (Illumina), followed by labeling with fluorescence by a single-base extension reaction. Fluorescent signals were read on an Illumina BeadStation GX scanner. Normalization and calculation of  $\beta$ -values, the ratio of methylated to unmethylated cytosine, was performed using GenomeStudio (Illumina). A  $\beta$ -value of 0 indicates nonmethylated cytosine, and that of 1 indicates fully methylated cytosine. The relative distance of the Infinium probe site from a region-of-interest, such as long-terminal repeat 7 (LTR7) and long-interspersed element-1 (LINE-1), was defined as the distance between the center of the region of interest and the probe position.

**Pyrosequencing.** Genomic DNA was extracted using a DNeasy Blood and Tissue Kit (Qiagen). Purified genomic DNA (500 ng) was used for bisulfite CT conversion with an EZ DNA methylation kit (Zymo Research). PCR was performed in a 25- $\mu$ L reaction mixture containing 25 ng of bisulfite-converted DNA, Pyromark PCR Master Mix (Qiagen), Coral Load Concentrate (Qiagen), and 0.3  $\mu$ M forward and 5' biotinylated reverse primers. PCR conditions were 45 cycles at 95 °C for 30 s, 50 °C for 30 s, and 72 °C for 30 s. The PCR product was bound to streptavidin Sepharose beads (Amersham Biosciences) and then purified, washed, denatured, and washed again. Then, 0.3  $\mu$ mol/L pyrosequencing primer was annealed to the purified PCR product. Pyrosequencing reactions were performed in the PSQ HS 96 Pyrosequencing System. The degree of methylation was expressed as the percentage of methylated cytosines divided by the sum of methylated and unmethylated cytosines. To validate the PCR pyrosequencing assay, each CpG dinucleotide position was assayed in triplicate and averages were used in the final analysis. The primer sequences are shown in [Dataset S3](#).

**Plasmid Construction.** To generate a doxycycline (Dox)-inducible KLF4 expression vector, the KLF4 ORF was cloned into PB/TA/ERN (10) using the Gateway LR reaction system (Life Technologies). Short hairpin RNA sequences were inserted into the AgeI/EcoRI site of pMKO.1-puro (11) (Addgene). To generate a shRNA expression vector for ESCs/iPSCs, a BglII/EcoRI fragment of each shRNA construct was transferred into the BamHI/MfeI site of PB/CAG-GIP/BP. All inserted fragments were verified by sequencing. Target sequences of shRNAs are as follows; LTR7-1 (CCT GTT TGG TGG TCT CTT CAC), LTR7-2 (TGT TTG GTG GTC TCT TCA CAC), long intergenic non-protein coding RNA, regulator of reprogramming (lincRNA-RoR) (AAG CCT GAG AGT TGG CAT GAA), and KLF4 (GAT CAA GCA GGA GGC GGTC TC).

**ChIP.** For the ChIP assay of exogenous reprogramming factors, such as OCT3/4, SOX2, and KLF4, 3× Flag-tagged factors or nontagged factors were transduced into HDFs using a PLAT-E-produced retroviral system. These cells were harvested at 3 d posttransduction. Cells were fixed with 1% formaldehyde and quenched with 125 mM glycine. Fixed cells were sequentially treated with LB1 [50 mM Hepes-KOH, pH 7.5, 140 mM NaCl, 1 mM EDTA, 10% (wt/vol) glycerol, 0.5% Nonidet-P 40, and 0.25% TritonX-100], LB2 (10 mM Tris-HCl, pH 8.0, 200 mM NaCl, 1 mM EDTA, and 0.5 mM EGTA), LB3 (10 mM Tris-HCl, pH 8.0, 100 mM NaCl, 1 mM EDTA, 0.5 mM EGTA, and 0.1% sodium deoxycholate) to obtain nuclear extracts. Chromatin samples were sheared by treatment with a Misonix Astrason S-3000 sonicator (ON, 30 s; OFF, 1 min; Power, 7.0; 15 cycles). A one-tenth volume of 10% (wt/vol) TritonX-100 solution was added to the cell lysates to obtain cleared supernatants after centrifugation. To reduce the nonspecific background, the chromatin samples were incubated with normal IgG (Santa Cruz) linked to Dynabeads (Life Technologies) for 30 min at 4 °C. After removal of the beads, the cleared lysates were incubated with a Dynabead-conjugated antibody overnight at 4 °C with constant rotation. After incubation, the beads were washed twice each with Wash buffer 1 (20 mM Tris-HCl, 8.0, 150 mM NaCl, 2 mM EDTA, 1% TritonX-100, and 0.1% SDS), wash buffer 2 (20 mM Tris-HCl, pH 8.0, 500 mM NaCl, 2 mM EDTA, 1% TritonX-100, and 0.1% SDS), wash buffer 3 (10 mM Tris-HCl, pH 8.0, 250 mM lithium chloride, 1 mM EDTA, 1% Nonidet-P 40, and 1% sodium deoxycholate), and TE buffer (10 mM Tris-HCl, pH 8.0 and 1 mM EDTA). The beads were then incubated with elution buffer (25 mM Tris-HCl, pH 7.5, 5 mM EDTA, and 0.5% SDS) supplemented with 0.4 mg/mL protease K (Nacalai tesque) at 42 °C for 1 h and then at 65 °C overnight with constant rotation. Eluates were purified using a Qiaquick PCR purification kit (Qiagen).

Multiplexed ChIP-seq libraries were prepared from 10 ng of immunoprecipitated DNA fragments using NEBNext ChIP-seq Library Prep Master Mix (New England BioLabs). For sequencing using GAIIx (Illumina), cluster generation was performed using TruSeq SR Cluster Kit v2 (Illumina). Each lane of flow cells contained one sample. Sequencing was performed in single-read run mode with a total 76 cycles, including a 75-bp read and one cycle for phasing. For sequencing using HiSeq2000 (Illumina), cluster generation was performed using TruSeq SR Cluster Kit v3 (Illumina) and six indexed libraries were loaded into each lane of flow cells. Sequencing was performed in multiplexed single-read run mode with total 86 cycles, including 6 cycles for reading the index sequence. Peak call was executed using a model-based analysis of the ChIP-seq algorithm (MACS) v1.4.0rc2 with default parameters.

**RNA-Seq Library Preparation and Sequencing.** DNase-treated RNA (100 ng) was used to prepare individually indexed and strand-specific RNA-seq libraries using a TruSeq Stranded Total RNA sample prep kit (Illumina). Briefly, ribosomal RNA was depleted using a Ribo-Zero Gold kit (AR Brown), followed by RNA fragmentation, cDNA synthesis, end repair, A-base addition, and ligation with Illumina-indexed adaptors. Cluster generation was performed using a TruSeq PE cluster Kit v3 on an Illumina cBot instrument. Six indexed libraries were loaded into each lane of flow cells. Sequencing was performed on a HiSeq2000 in multiplexed paired-read run mode with a total of 208 cycles, including 6 cycles for reading the index sequence.

**Data Analysis of Deep Sequencing.** Conversion of Bcl into Fastq format was achieved using the configureBclToFastq.pl program, a part of CASAVA 1.8.2 (Illumina). Sequence reads were then aligned to the human genome (GRCh37/hg19) using the paired-end mode of the BWA v0.5.9rc1 and SAMtools v0.1.17 (ChIP-seq), or TopHat2 software (RNA-seq). Aligned sequence tags were visualized using GenomeJack v2.1 (Mitsubishi Space Software).



**Quantitative Expression Analysis of Repeat Sequences.** RepeatMasker open-3.3.0 ([www.repeatmasker.org](http://www.repeatmasker.org)), a database of human repetitive sequences, was applied to reference sequences of LTR7 and LINE-1. The LTR7 sequence was from LTR/endogenous retrovirus (ERV)-1 in the database, including LTR7, LTR7A, LTR7B, LTR7C, and LTR7Y, and 3771 LTR7 regions were found. The number of LINE-1 regions (LINE/L1 in the database) was 979,568. For RNA-seq, the number of sequence reads aligned with the LTR7-coding region by TopHat2 was counted using the Partek Genomics Suite. Sample-to-sample variation was normalized as follows: normalized number of sequence tags on LTR7 = number of reads aligned with the LTR7 region/total number of hg19-mappable sequence tags.

**Single-Cell Expression Analysis.** Single-cell suspensions prepared by treatment with 0.25% trypsin/1 mM EDTA were incubated with PE-conjugated TRA-1-60 and DAPI. TRA-1-60 (+)/DAPI (-) cells were directly sorted into PCR master mix using the FACS Aria II. The template for single-cell PCR was prepared using CellsDirect reagent (Life Technologies). Pre-amplification of the target sequences was performed for 22 cycles. Subsequent PCR

and data collection were conducted with a Biomark system (Fluidigm). Each sample was validated based on expression of *G3PDH* or *ACTB*, with a Ct value < 15. Ct values > 26 were taken to indicate no expression and were unified as 100 for calculation of  $\Delta$ Ct. We used following Taqman assays; abhydrolase domain containing 12B (*ABHD12B*) (Hs00997975\_g1), HERV-H LTR-associating 1 (*HHLAI*) (Hs00903176\_g1) and chromosome 4 open reading frame 51 (*C4ORF51*) (Hs03037752\_m1).

**Southern Blotting.** Genomic DNA (3–5  $\mu$ g) was digested with restriction enzymes overnight. Digested DNA were separated on a 0.8% agarose gel and transferred to a nylon membrane (Amersham Biosciences). The membrane was incubated with digoxigenin (DIG)-labeled DNA probe in DIG Easy Hyb buffer (Roche) at 42 °C overnight with constant rotation. After washing, alkaline phosphatase-conjugated anti-DIG antibody (1:10,000; Roche) was added to the membrane. Signals were produced with CDP-star reagent (Roche) and detected using a LAS3000 imaging system (Fuji Film). Primer sequences for generation of probes are shown in [Dataset S3](#).

1. Morita S, Kojima T, Kitamura T (2000) Plat-E: An efficient and stable system for transient packaging of retroviruses. *Gene Ther* 7(12):1063–1066.
2. Thomson JA, et al. (1998) Embryonic stem cell lines derived from human blastocysts. *Science* 282(5391):1145–1147.
3. Suemori H, et al. (2006) Efficient establishment of human embryonic stem cell lines and long-term maintenance with stable karyotype by enzymatic bulk passage. *Biochem Biophys Res Commun* 345(3):926–932.
4. Takahashi K, et al. (2007) Induction of pluripotent stem cells from adult human fibroblasts by defined factors. *Cell* 131(5):861–872.
5. Tanabe K, Nakamura M, Narita M, Takahashi K, Yamanaka S (2013) Maturation, not initiation, is the major roadblock during reprogramming toward pluripotency from human fibroblasts. *Proc Natl Acad Sci USA* 110(30):12172–12179.
6. Takahashi K, et al. (2014) Induction of pluripotency in human somatic cells via a transient state resembling primitive streak-like mesendoderm. *Nat Commun* 5:3678.
7. Oldershaw RA, et al. (2010) Directed differentiation of human embryonic stem cells toward chondrocytes. *Nat Biotechnol* 28(11):1187–1194.
8. Kajiwarra M, et al. (2012) Donor-dependent variations in hepatic differentiation from human-induced pluripotent stem cells. *Proc Natl Acad Sci USA* 109(31):12538–12543.
9. Mae S, et al. (2013) Monitoring and robust induction of nephrogenic intermediate mesoderm from human pluripotent stem cells. *Nat Commun* 4:1367.
10. Woltjen K, et al. (2009) piggyBac transposition reprograms fibroblasts to induced pluripotent stem cells. *Nature* 458(7239):766–770.
11. Masutomi K, et al. (2003) Telomerase maintains telomere structure in normal human cells. *Cell* 114(2):241–253.

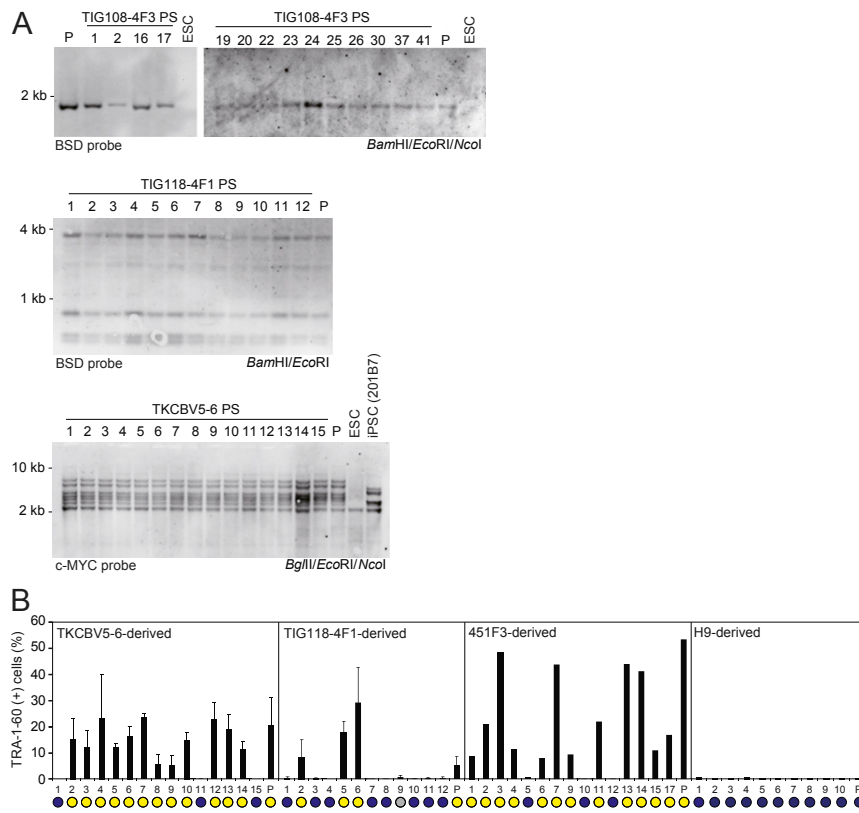


**Fig. S1.** Subcloning of DD-iPSCs. **(A)** Monoclonal origin of iPSC subclones. The genomic DNA of the subclones derived from TKCBV5-6, TIG108-4F3, and TIG118-4F1 by Southern blotting. Restriction enzymes and probes used for each clone are shown. For subclones derived from the 451F3 integration-free iPSC clone, short tandem-repeat analyses were performed for 16 loci (D3S1358, TH01, D21S11, D18S51, Penta\_E, D5S818, D13S317, D7S820, D16S539, CSF1PO, Penta\_D, AMEL, vWA, D8S1179, TPOX, and FGA). **(B)** Percentages of TRA-1-60 (+) cells 14 d after neural induction of each primary subclone and parental cells (P) analyzed by flow cytometry. Blue and yellow circles indicate normal and DD-iPSC subclone, respectively.  $n = 2-3$ . Error bars are SDs.



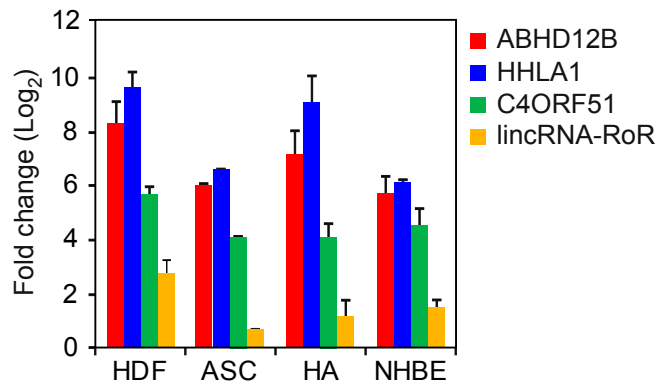


**Fig. 53.** The expression of DD-iPSC markers in TRA-1-60 (+) cells from various origins. Fold-increases of *ABHD12B*, *HHLA1*, *C4ORF51*, and *lincRNA-RoR* expression in TRA-1-60 (+) intermediate reprogrammed cells on day 28 compared with original somatic cell lines, determined by microarray. ASC, adipose tissue-derived mesenchymal stem cells; HA, human astrocytes; NHBE, normal human bronchial epithelium.  $n = 3$ . Error bars are SDs.

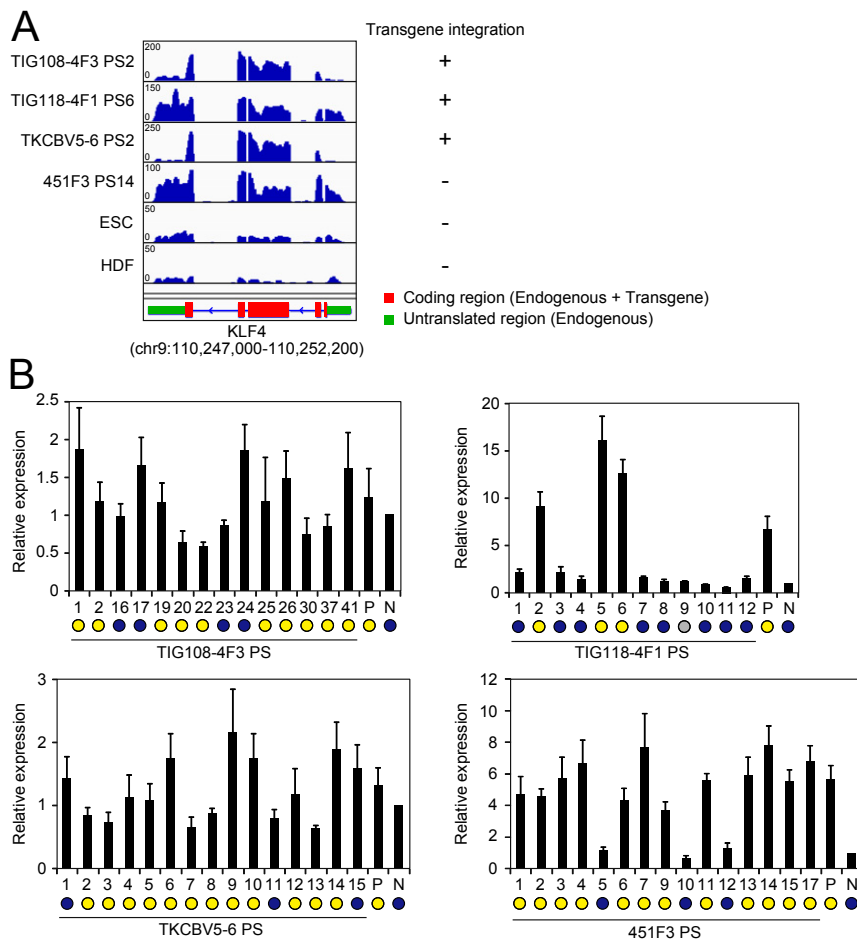


**Fig. 54.** *KLF4* transcripts in DD-iPSCs. (A) The histogram shows the representative transcription patterns of *KLF4* in DD-iPSC primary subclones (PS), ESCs, and HDFs analyzed by RNA-seq. Red and green box indicate protein coding region (common in transgene and endogenous locus) and untranslated region (only in endogenous locus), respectively. (B) The relative expression of endogenous *KLF4* in DD-iPSCs and their primary subclones (PS) compared with those in normal iPSCs (N) analyzed qRT-PCR. Blue and yellow circles indicate normal and DD-iPSC subclones/parents, respectively.  $n = 3$ . Error bars are SDs.

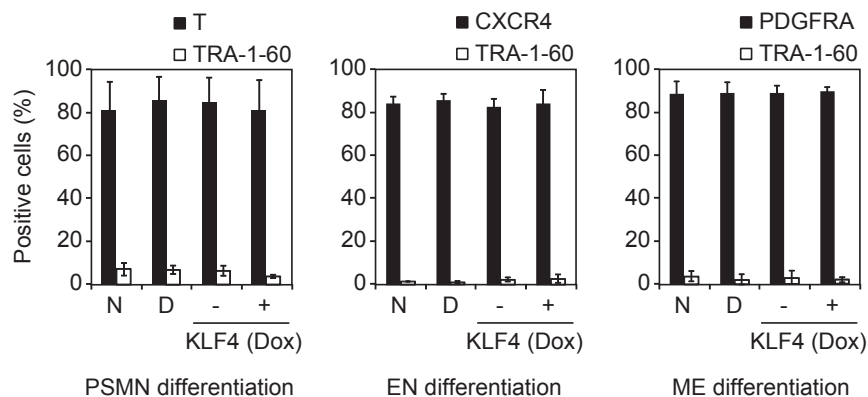


**Fig. S5.** Differentiation potential of DD-iPSCs and KLF4-overexpressing iPSCs. Normal iPSCs (N), DD-iPSCs (D), and normal iPSCs transduced with Dox-inducible KLF4 were differentiated into primitive streak-like mesendoderm (PSMN), endoderm (EN), or mesoderm (ME) in the conditions with (+) or without (-) Dox. Closed bars in each graph represent the differentiation efficiencies into PSMN, EN, and ME evaluated by immunostaining with T, CXCR4, and PDGFRA, respectively. Open bars indicate the percentages of residual undifferentiated cells labeled by TRA-1-60.  $n = 3$ . Error bars are SDs.

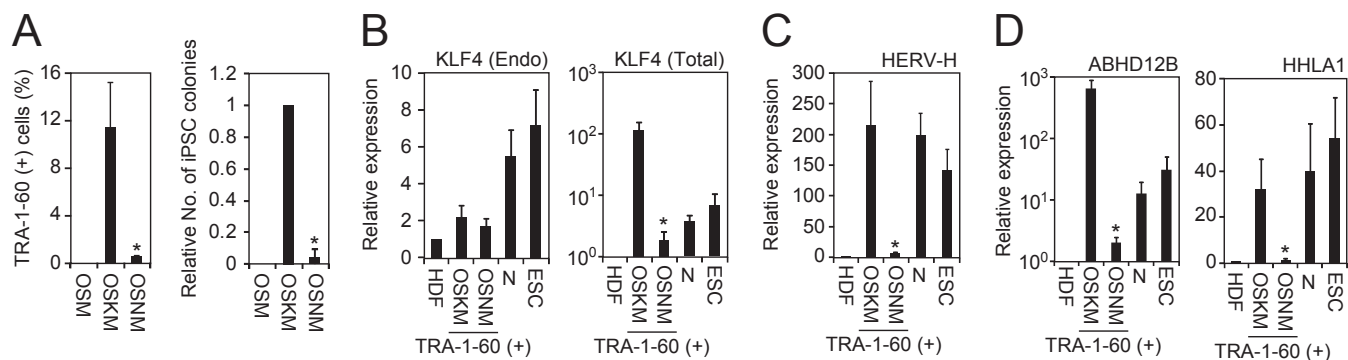


**Fig. S6.** The effect of exogenous NANOG homeobox (NANOG) on human ERV-H (HERV-H) activity. (A) Low reprogramming activity of NANOG. Shown are the proportion of TRA-1-60 (+) cells on day 7 posttransduction of indicated factors (Left) and relative numbers of iPSC colonies counted on day 28 compared with those induced by OCT3/4, SOX2, KLF4, and c-MYC (OSKM) (Right). Error bars are SD.  $n = 3$ . \* $P < 0.05$  vs. OSKM was calculated by  $t$  test. (B) NANOG does not enhance KLF4 expression. Shown are the relative expression of endogenous (Endo) and total KLF4 in HDFs, TRA-1-60 (+) cells induced by OSKM or OSNM (OSM with NANOG instead of KLF4) on day 7, normal iPSCs (N), and ESCs compared with those in HDFs, revealed by qRT-PCR. Each value was normalized to that of *G3PDH*.  $n = 3$ . Error bars are SD. \* $P < 0.05$  vs. OSKM was calculated by  $t$  test. (C) Low activity of NANOG for HERV-H induction. Shown are the relative expression of HERV-H in HDFs, TRA-1-60 (+) cells induced by OSKM or OSNM on day 7, normal iPSCs (N), and ESCs compared with those in HDFs, revealed by qRT-PCR. Each value was normalized to that of *G3PDH*, and then the value of Mock was adjusted to be 1.  $n = 3$ . Error bars are SD. \* $P < 0.05$  vs. OSKM was calculated by  $t$  test. (D) NANOG slightly enhanced the expression of LTR7-related genes. Shown are the relative expressions of LTR7-related genes *ABHD12B* and *HHLA1* in HDFs, TRA-1-60 (+) cells induced by OSKM or OSNM on day 7, normal iPSCs (N), and ESCs compared with those in HDFs, revealed by microarray.  $n = 3$ . Error bars are SD. \*FDR  $< 0.05$  vs. OSKM was calculated by  $t$  test.

#### Dataset S1. Short tandem-repeat analyses of 451F3 subclones

##### Dataset S1

Shown are the results of short tandem-repeat analyses for 16 loci (D3S1358, TH01, D21S11, D18S51, Penta\_E, D5S818, D13S317, D7S820, D16S539, CSF1PO, Penta\_D, AMEL, vWA, D8S1179, TPOX, and FGA) in 451F3 integration-free parental iPSCs (P) and its primary subclones (PS).

#### Dataset S2. DD-iPSC markers

##### Dataset S2

Microarray probes, genomic location, and gene symbols of DD-iPSC marker genes,  $P$  values and fold-change (FC) for comparison between normal and DD-iPSC subclones.

### Dataset S3. Primer sequences used in the study

#### [Dataset S3](#)

The purposes, targets and sequences of primers used in this study are listed.